International Journal of Microwave and Wireless Technologies

cambridge.org/mrf

Analysis of Fabry–Perot cavity antennas based on thick partially reflecting sheets through a field matching technique

Edoardo Negri[1], Walter Fuscaldo[1], Paolo Burghignoli[2] and Alessandro Galli[2]

[1]Istituto per la Microelettronica e Microsistemi, Consiglio Nazionale delle Ricerche, Rome, Italy and [2]Department of Information Engineering, Electronics and Telecommunications, Sapienza University of Rome, Rome, Italy

Research Paper

Cite this article: Negri E, Fuscaldo W, Burghignoli P, Galli A (2025) Analysis of Fabry–Perot cavity antennas based on thick partially reflecting sheets through a field matching technique. *International Journal of Microwave and Wireless Technologies* **17**(9), 1516–1523. https://doi.org/10.1017/S1759078725102432

Received: 30 January 2025
Revised: 29 September 2025
Accepted: 6 October 2025

Keywords:
Fabry–Perot cavity antennas; field matching technique; leaky waves; matching technique; partially reflecting sheets

Corresponding author: Edoardo Negri;
Email: edoardonegri@cnr.it

Abstract

An original analysis of Fabry–Perot cavity antennas based on thick partially reflecting sheet (PRS) is presented in this work. The bandwidth enhancement of such radiating devices with respect to Fabry–Perot cavity antennas based on thin PRS has been investigated through a leaky-wave, transverse-equivalent-network approach, and a field matching technique. This analysis led to an optimal condition for considerably improving the gain-bandwidth figure of merit for this class of radiating devices on a sound physical basis. A Fabry–Perot cavity antenna based on a thick PRS working at 60 GHz is discussed as a case study. An excellent impedance matching is finally achieved by means of an efficient feeding network designed through a fast ad hoc, hybrid, analytical-numerical method. Theoretical results are in an excellent agreement with full-wave simulations corroborating the proposed methods.

Introduction

An earlier version of this paper was presented at the 54 European Microwave Conference (EuMC 2024) and was published in its Proceedings [1] where we preliminarily analyzed the evolution of leaky modes in Fabry–Perot cavity antennas (FPCAs) based on thin and thick partially reflecting sheets (PRSs). The content of [1] is extended in this paper by deeply investigating a field-matching-technique (FMT) approach to analyze and describe this kind of radiating structures. Moreover, a realistic implementation of the considered leaky-wave antenna has been designed with a rectangular-waveguide feeder, impedance-matched through an efficient semi-analytical approach.

As previously discussed in [1], FPCAs provide a simple yet effective solution to the long-standing problem of a simultaneously highly directive and low-profile radiating device [2]. These characteristics are crucial in different application contexts, such as advanced terrestrial [3, 4] and satellite communications [5].

Fabry–Perot cavity antennas share a common architecture that consists in a grounded dielectric slab with a PRS on top [6]. Such devices can simply be fed by *vertical* electric/magnetic dipoles (VEDs/VMDs), which excite an azimuthally symmetric transverse magnetic/electric (TM/TE) leaky mode. In this manner, an omnidirectional conical beam with scanning capabilities is achieved although it is not possible to radiate at broadside due to the null enforced by the source symmetry [2, 7]. For this reason, in order to obtain a pencil beam at broadside, FPCAs are excited with a *horizontal* electric or magnetic dipole (HED or HMD), which is constituted by a bent coaxial cable (L-probe) [8, 9] or a quasi-resonant slot on the ground plane [10], respectively. However, in this case, an omnidirectional conical beam can no longer be guaranteed, unless specific metasurfaces or metamaterials are used [11, 12]. Due to the fragility of coaxial cables as the frequency increases [13], (sub)millimeter-wave FPCAs are preferably fed by a rectangular slot on the ground plane excited by a rectangular waveguide [6] (such a solution can be extended up to the THz frequency range [14–16]). In this paper, moreover, an efficient semi-analytical matching technique has been exploited to design two capacitive irises inside the rectangular-waveguide feeder of the proposed leaky-wave antenna [17].

As concerns the PRS implementation, the typical solution is given by a *thin* isotropic metasurface, i.e., a patterned metal sheet whose periodicity is much smaller than the operative wavelength [18]. Common examples are metal strip gratings and patch arrays [19], although it has recently been proven that a fishnet unit cell provides more degrees of freedom and is more suitable for high-frequency (viz., THz) designs [6]. Such structures are usually realized through low-cost, large-area, photolithographic techniques with a resolution down to 3 μm. The latter ensures the repeatability and accuracy of the PRS physical implementation up to THz frequencies [20]. By assuming an ideal metal, i.e., a perfect electric conductor (PEC), a thin PRS

© The Author(s), 2025. Published by Cambridge University Press in association with The European Microwave Association. This is an Open Access article, distributed under the terms of the Creative Commons Attribution-NonCommercial-NoDerivatives licence (http://creativecommons.org/licenses/by-nc-nd/4.0), which permits non-commercial re-use, distribution, and reproduction in any medium, provided that no alterations are made and the original article is properly cited. The written permission of Cambridge University Press must be obtained prior to any commercial use and/or adaptation of the article.

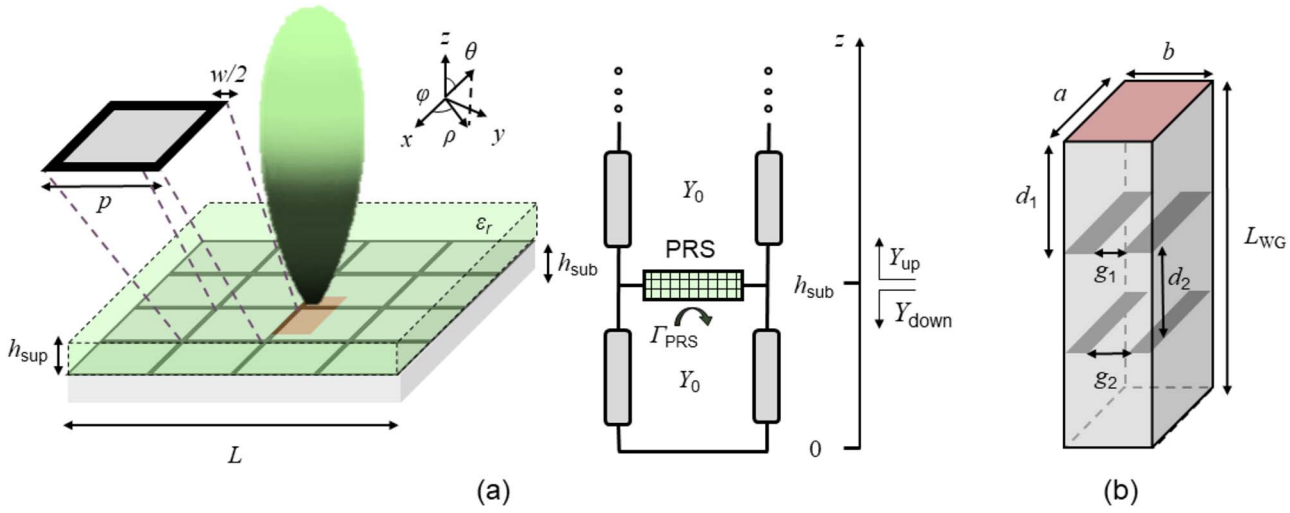


Figure 1. (a) Schematic representation of a Fabry–Perot cavity antenna, its thin-PRS unit cell, and its broadside pencil-beam radiation pattern. While the gray solid describes the air-filled cavity, the black color shows the perfect electric conductor which is used to implement the thin-PRS metallic pattern. The semi-transparent green solid box describes the dielectric superstrate which is present only for Fabry–Perot cavity antennas based on thick PRSs. The red rectangular area shows the slot on the ground plane fed by the rectangular waveguide. On the right, the TEN of the device is reported. The PRS contribution, both in the *thin* and in the *thick* cases, is described by the reflection coefficient Γ_{PRS} of the PRS looking upwards from the cavity. (b) Rectangular-waveguide feeder and its matching network constituted by two capacitive irises with their relevant design parameters. The red area on top represents the section at which the source is connected to the Fabry–Perot cavity antenna.

can be represented through a scalar, purely imaginary, equivalent impedance sheet $Z_s = jX_s$ [6, 18, 19] (such hypothesis has been experimentally demonstrated also in the THz band [20]).

As is well-known [21], FPCAs become more directive (with the drawback of a lower bandwidth) as the reflectivity of the PRS increases and, thus, as $X_s \to 0$. In particular, for an air-filled cavity with a thin PRS on top, it is seen that the figure of merit given by the product of the directivity and the fractional bandwidth is constant and equal to 2.47 [22]. This aspect is related to the resonance condition of FPCAs (see, e.g., [23]), which is exactly satisfied for a single frequency due to the *Foster*-like behavior [24] of a thin PRS [1]. Such a narrowband characteristic has been mitigated by optimizing the PRS design with different approaches, such as genetic algorithms [3], double-layer PRS metasurfaces [25], and multi-layer structures [26, 27].

One of the most promising solutions is given by *thick* PRSs [28] which are constituted by an isotropic metallic metasurface with a dielectric superstrate on top. By properly designing the superstrate height h_{sup}, it is possible to achieve a *non-Foster*-like response of the thick PRS which is related to the presence of a positive slope of the phase of the reflection coefficient of the PRS, Γ_{PRS} [29]. In this manner, it is possible to properly design the PRS to closely fulfill the cavity resonance condition over a wider frequency region with respect to the thin PRS case, and thus improve the FPCA gain-bandwidth figure of merit [29].

In the literature, the design of thick PRSs has been addressed through a combined leaky-wave and full-wave approach. In particular, the contribution of the PRS in the transverse equivalent network (TEN) of the FPCA – which is used for retrieving the leaky-mode dispersion curves through the transverse resonance technique [30] – has been described through the evaluation of its reflection coefficient with commercial solvers [29]. Here, as in the previous version of this paper [1], a FMT is exploited for retrieving the variation of the behavior of leaky modes when the device changes from a *thin* to a *thick* PRS with different superstrate thicknesses. This analysis demonstrates that the bandwidth enhancement in these radiating devices occurs because of an additional resonance of the leaky mode in the superstrate. Moreover, in this paper, the considered FPCA based on a thick PRS has been simulated and fed through a realistic rectangular-waveguide source matched by means of a semi-analytical approach [17].

The paper is organized as follows. In second section, the theoretical background related to FPCAs based on thick PRS is briefly reported by showing the optimal choice of the cavity height h_{sub}, the TEN of the device, and the dispersion analysis of the leaky modes. In Section "Field matching technique", the FMT is presented and exploited to describe how the leaky-mode field distributions change as the cavity parameters vary. In Section "Full-wave analysis", the model of the proposed device is implemented on a full-wave solver with a realistic feeder to corroborate the far-field results. Conclusions are finally drawn in last section.

Theoretical background

Fabry–Perot cavity antennas have been studied with different approaches, such as the ray-optics model [23], the application of the reciprocity theorem on their equivalent transmission line [21], and the leaky-wave perspective [2]. Regardless the considered method, the most important design rule in FPCAs is related to the proper choice of the cavity height h as a function of X_s and the working frequency f with the aim of maximizing the radiated power on a certain direction θ_0. For an air-filled cavity pointing at broadside, i.e., with $\theta_0 = 0$, it results [23]:

$$h(f) = \frac{\lambda_0}{4\pi}\left[\phi_{PRS}(f) - \pi(2n-1)\right], \; n = 0, \pm 1, \ldots, \qquad (1)$$

where λ_0 is the vacuum wavelength at the frequency f and ϕ_{PRS} is the phase of the reflection coefficient seen from the ground plane, i.e., $\Gamma_{PRS} = |\Gamma_{PRS}|e^{j\phi_{PRS}}$ (see Fig. 1). The evaluation of the Γ_{PRS} value can be addressed in any commercial solver by considering

https://doi.org/10.1017/S1759078725102432 Published online by Cambridge University Press

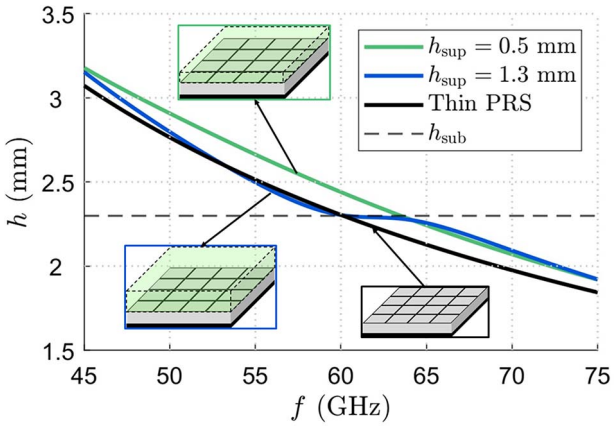


Figure 2. Cavity height h which satisfies the resonance condition (1) vs. frequency f in the presence of a thin PRS (black solid line) or of a thick PRS with $h_{sup} = 0.5$ mm (green solid line) or $h_{sup} = 1.3$ mm (blue solid line). The thin, black, dashed horizontal line represents the substrate height $h_{sub} = 2.3$ mm chosen in this work. The insets pictorially show the device for each configuration.

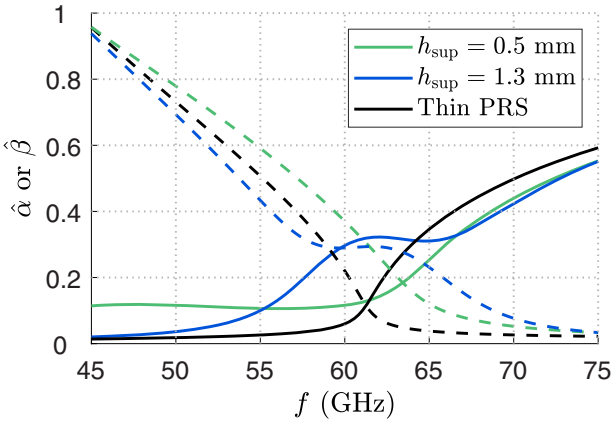


Figure 3. Dispersion curves vs. frequency f of the leaky-wave phase (solid lines) and attenuation (dashed lines) constants normalized with respect to the vacuum wavenumber k_0, i.e., $\hat{\beta} = \beta/k_0$, and $\hat{\alpha} = \alpha/k_0$, respectively. The cases of a thin PRS, a thick PRS with $h_{sup} = 0.5$ mm, and a thick PRS with $h_{sup} = 1.3$ mm are reported in black, green, and blue curves, respectively.

the simulation of the unit cell in a periodic environment (see e.g., [6, 29] for further details).

In this paper, a metal strip grating with periodicity $p = \lambda_0/6$ and strip width $w = 0.125p$ is considered (see Fig. 1), obtaining $X_s \simeq 100\ \Omega$ (in good agreement with homogenization formulas in [19]). The reflection coefficient Γ_{PRS} at the substrate-air interface has been retrieved for three different examples in the 45–75 GHz frequency range through a frequency-domain simulation on CST Microwave Studio [31]: the case of the simple *thin* PRS, and a pair of *thick*-PRS configurations realized through the same metal strip grating with a lossless superstrate on top whose relative permittivity is $\varepsilon_r = 6.15$ and whose heights are $h_{sup} = 0.5$ mm or $h_{sup} = 1.3$ mm. This dielectric choice is representative of a realistic Rogers TC600 laminate which presents the same relative permittivity ε_r with a negligible, loss-tangent value of $\tan\delta = 0.002$.

As one can infer from Fig. 2, the curve of the optimal substrate height h in the case of the *thin*-PRS case and the case of a *thick* PRS with $h_{sup} = 0.5$ mm intersects the design substrate height $h_{sub} = 2.3$ mm only at a single frequency. This condition results from the Foster-like behavior of the phase of the reflection coefficient ϕ_{PRS}, viz. $\partial\phi_{PRS}/\partial f < 0$. In order to enhance the device working bandwidth, the condition (1) has to be satisfied over a wide frequency range. For this reason, a *thicker* superstrate (viz., $h_{sup} = 1.3$ mm) has been placed above the thin PRS, obtaining a *thick* PRS with a *non-Foster* behavior. Interestingly, this phase envelope is present only near the condition $h_{sup} \simeq \lambda_d/2$ (with λ_d being the operative wavelength in the dielectric superstrate) and not for a thinner or thicker superstrate. As shown in Fig. 2, equation (1) is now satisfied over a wide frequency range for a substrate height $h = h_{sub} = 2.3$ mm (the relevant curve of h has a flat behavior vs. f around 60 GHz), leading to the desired wide bandwidth.

At this point, it is worth noting that in FPCAs based on thin [2] or thick [29] PRS, the radiating features – such as the radiation pattern, the directivity, and the bandwidth – can be predicted through the evaluation of the *leaky radial wavenumber* $k_\rho = \beta - j\alpha$ (with β and α being the leaky phase and attenuation constants, respectively). This task can be addressed by numerically solving the dispersion equation [32] obtained by applying the transverse resonance technique [30] to the TEN of the device. For the considered structures the dispersion equation reads (see Fig. 1):

$$Y_{up} + Y_{down} = Y_{up} - jY_0 \cot(k_z h_{sub}) = 0, \tag{2}$$

where Y_0 is the wave admittance of the substrate transmission line and $k_z = \sqrt{k_0^2 - k_\rho^2}$ its propagation constant (being k_0 the vacuum wavenumber). The value Y_{up} represents the admittance of the PRS looking upwards from the cavity, thus, it can easily be retrieved through the full-wave evaluation of the reflection coefficient Γ_{PRS} for a normal incidence (which represents with a good approximation the PRS behavior for low-angle oblique incidences):

$$Y_{up} = Y_0 \frac{1 - \Gamma_{PRS}}{1 + \Gamma_{PRS}}. \tag{3}$$

The results of the proposed analysis are shown in Fig. 3, where the leaky phase and attenuation constants are reported normalized with respect to the vacuum wavenumber with $\hat{\beta} = \beta/k_0$ and $\hat{\alpha} = \alpha/k_0$, respectively. It is worthwhile to point out that, as theoretically expected from the ray-optics approximation in (1) and shown in Fig. 2, the condition for which occurs the maximum radiated power at broadside, i.e., $\beta \simeq \alpha$ [33], is verified just at a single frequency for the case of a *thin* PRS and the case of a PRS which is *not thick enough* ($h_{sup} = 0.5$ mm). On the other hand, for a properly designed thick PRS with $h_{sup} = 1.3$ mm, the leaky phase β and attenuation α constants are very similar to each other over a wider frequency range, thus obtaining a theoretically wider −3 dB gain bandwidth.

Field matching technique

In this section, the leaky modes in an FPCA transitioning from a thin- to a thick-PRS case are investigated through an FMT approach. Without loss of generality, we assume the FPCA excited by an HMD source aligned with the x-axis, and we obtain the tangential electromagnetic fields over the E-plane, $\phi = 90°$. We recall that this source excites a purely TM_z (TE_z) electromagnetic field over the E-plane (H-plane) [34]. Thanks to the geometry of the problem, as shown in [1], the electric-field modal solution for an FPCA based on a *thin* PRS can be written as:

$$\begin{cases} E_\rho(z) = A_2 e^{-jk_z(z-h_{sub})}, & z > h_{sub} \\ E_\rho(z) = A_1 \sin(k_z z), & z \le h_{sub} \end{cases} \tag{4}$$

https://doi.org/10.1017/S1759078725102432 Published online by Cambridge University Press

where A_1 and A_2 are complex amplitude coefficients. This is due to the propagative nature of the electric field above the PRS (for $z \geq h_{\text{sub}}$) and its resonant behavior in the FPCA (for $z \leq h_{\text{sub}}$) with a null on the ground plane at $z = 0$. At this point, from Maxwell's equations, the magnetic field reads:

$$\begin{cases} H_\phi(z) &= Y_0 A_2 e^{-jk_z(z-h_{\text{sub}})}, \quad z > h_{\text{sub}} \\ H_\phi(z) &= jY_0 A_1 \cos(k_z z), \quad z \leq h_{\text{sub}} \end{cases} \tag{5}$$

By applying the boundary conditions at $z = h_{\text{sub}}$ related to the homogenized metasurface representing the PRS (viz., $E_\rho(z = h_{\text{sub}}^-) = E_\rho(z = h_{\text{sub}}^+)$ and $H_\phi(z = h_{\text{sub}}^+) - H_\phi(z = h_{\text{sub}}^-) = Y_s E_\rho(z = h_{\text{sub}})$), the problem can be recast in the following matrix form:

$$\begin{bmatrix} \sin(k_z h) & -1 \\ -jY_0 \cos(k_z h) + Y_s \sin(k_z h) & Y_0 \end{bmatrix} \begin{bmatrix} A_1 \\ A_2 \end{bmatrix} = 0, \tag{6}$$

with $Y_s = 1/Z_s$ being the equivalent admittance sheet of the PRS. A nontrivial solution for (6) is obtained by enforcing the determinant to zero, which yields the determinantal equation (note that the analogous formula, i.e. (7) of [1], has an incorrect sign of the second addend):

$$Y_0 + Y_s - jY_0 \cot(k_z h) = 0, \tag{7}$$

which is equivalent to (2), since $Y_{\text{up}} = Y_0 + Y_s$, but a full-wave simulation is not needed for the evaluation of Γ_{PRS}. It is worthwhile to note that, assuming an Y_s dependent on θ, this approach is valid for any angle of incidence. Moreover, by considering PRS unit-cell configurations that are almost spatially nondispersive [6], a constant Y_s value for different incident angles can be assumed, still providing a valid antenna model. Equation (7) can then be numerically solved [32], obtaining the same leaky wavenumbers of "Theoretical background" section. In addition, the leaky-wave fields can be determined by solving for the unknown coefficients in (6). (The two equations are linearly dependent, so one of the two coefficients is arbitrarily set to unity and the reduced system solved for the other coefficient.)

A similar FMT approach can be repeated to obtain the leaky-wave fields for the *thick*-PRS case. By following the same procedure of the thin-PRS structure but assuming the presence of an additional layer, one has the following magnetic-field distribution:

$$\begin{cases} H_\phi(z) &= A_1 e^{-jk_{z0}(z-h_{\text{tot}})}, \quad z \geq h_{\text{tot}} \\ H_\phi(z) &= A_2 \cos[k_{zd}(z-h_{\text{sub}})] + \\ & \quad A_3 \sin[k_{zd}(z-h_{\text{sub}})], \quad h_{\text{sub}} < z < h_{\text{tot}} \\ H_\phi(z) &= A_4 \cos(k_{z0} z), \quad 0 \leq z \leq h_{\text{sub}}, \end{cases} \tag{8}$$

where $h_{\text{tot}} = h_{\text{sub}} + h_{\text{sup}}$ is the total device height, $k_{z0} = \sqrt{k_0^2 - k_\rho^2}$, and $k_{zd} = \sqrt{\varepsilon_r k_0^2 - k_\rho^2}$ are the propagation constants in the vacuum and dielectric, respectively.

By applying Maxwell's equation for this TM-polarized field, one can retrieve the electric-field distribution as:

$$\begin{cases} E_\rho(z) &= Z_0 A_1 e^{-jk_{z0}(z-h_{\text{tot}})}, \quad z \geq h_{\text{tot}} \\ E_\rho(z) &= jZ_d\{A_3 \cos[k_{zd}(z-h_{\text{sub}})] - \\ & \quad A_2 \sin[k_{zd}(z-h_{\text{sub}})]\}, \quad h_{\text{sub}} < z < h_{\text{tot}} \\ E_\rho(z) &= -jZ_0 A_4 \sin(k_{z0} z), \quad 0 \leq z \leq h_{\text{sub}}, \end{cases} \tag{9}$$

where $Z_0 = k_{z0}/(\omega\varepsilon_0) = 1/Y_0$ and $Z_d = k_{zd}/(\omega\varepsilon_r\varepsilon_0)$.

At this point the boundary conditions have to be enforced. In particular, while the continuity of the tangential components of the electric and magnetic field has to be considered in $z = h_{\text{tot}}$, only the tangential electric field is invariant at $z = h_{\text{sub}}$. As for the 'thin' case, this aspect is due to the presence of the PRS which enforces the discontinuity of the tangential magnetic field components caused by an induced current as $\mathbf{J}_s = Y_s \mathbf{E}_\rho = \mathbf{z} \times (\mathbf{H}^+ - \mathbf{H}^-)$. In this manner, a system with four equations and four unknowns is obtained and reported in its matrix form:

$$\begin{bmatrix} 1 & -\cos(k_{zd}h_{\text{sup}}) & -\sin(k_{zd}h_{\text{sup}}) & \cdots & 0 \\ Z_0 & jZ_d \sin(k_{zd}h_{\text{sup}}) & -jZ_d \cos(k_{zd}h_{\text{sup}}) & & 0 \\ 0 & 0 & jZ_d & & 0 \\ 0 & 1 & jZ_d Y_s & & jZ_0 \sin(k_{z0}h_{\text{sub}}) \\ & & & & -\cos(k_{z0}h_{\text{sub}}) \end{bmatrix} \begin{bmatrix} A_1 \\ A_2 \\ A_3 \\ A_4 \end{bmatrix} = 0 \tag{10}$$

This system has a nontrivial solution only if the determinant is set to zero. As for the thin PRS case, it is thus possible to retrieve the dispersion equation of the structure without full-wave simulations. After few mathematical steps and by indicating $Y_d = 1/Z_d$, the determinantal equation reads:

$$Y_s + Y_d \frac{Y_0 + jY_d \tan(k_{zd}h_{\text{sup}})}{Y_d + jY_0 \tan(k_{zd}h_{\text{sup}})} - jY_0 \cot(k_{z0}h_{\text{sub}}) = 0. \tag{11}$$

It is worth noting that equation (11) is crucial for further studies and optimization procedures in FPCAs since it provides for the first time the dispersion analysis of these structures without requiring a full-wave simulation of the thick-PRS behavior.

When (11) is satisfied, all the equations in (10) are not independent. It is thus possible, for instance, to remove the first row and assume $A_1 = 1$. In this way, one has:

$$\begin{bmatrix} jZ_d \sin(k_{zd}h_{\text{sup}}) & -jZ_d \cos(k_{zd}h_{\text{sup}}) & \cdots & 0 \\ 0 & jZ_d & & jZ_0 \sin(k_{z0}h_{\text{sub}}) \\ 1 & jZ_d Y_s & & -\cos(k_{z0}h_{\text{sub}}) \end{bmatrix} \begin{bmatrix} A_2 \\ A_3 \\ A_4 \end{bmatrix} = \begin{bmatrix} -Z_0 \\ 0 \\ 0 \end{bmatrix} \tag{12}$$

By inverting the matrix in (12), the coefficient are determined as shown in (13), thus achieving the complete field-distribution evaluation.

$$\begin{cases} A_4 &= \{-j \sin(k_{z0}h_{\text{sub}}) \cos(k_{zd}h_{\text{sup}}) + \\ & \quad + \frac{Z_d}{Z_0} \sin(k_{zd}h_{\text{sup}})[-j \cos(k_{z0}h_{\text{sub}}) + \\ & \quad + Z_d Y_s \sin(k_{z0}h_{\text{sub}})]\}^{-1} \\ A_3 &= -A_4 \frac{Z_0}{Z_d} \sin(k_{z0}h_{\text{sub}}) \\ A_2 &= A_4 [\cos(k_{z0}h_{\text{sub}}) + jZ_0 Y_s \sin(k_{z0}h_{\text{sub}})] \end{cases} \tag{13}$$

https://doi.org/10.1017/S1759078725102432 Published online by Cambridge University Press

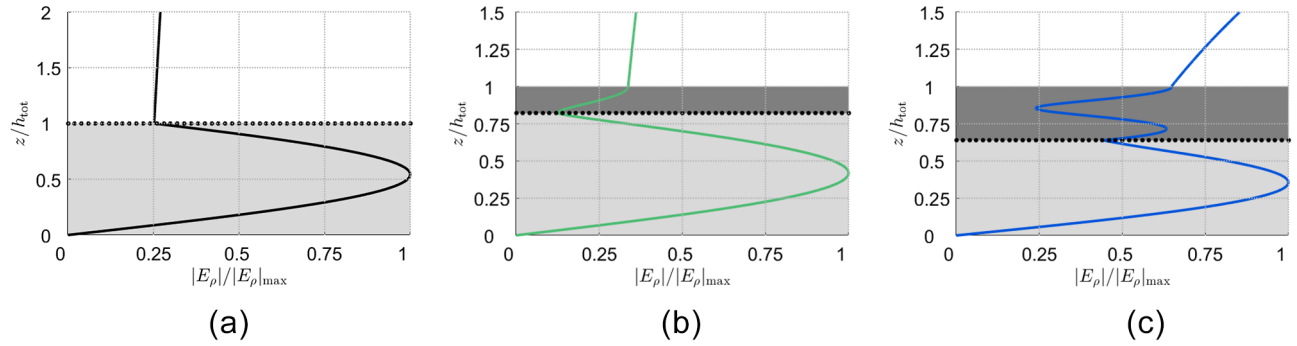


Figure 4. Results of the FMT analysis when (a) a thin PRS, (b) a thick PRS with $h_{\text{sup}} = 0.5$ mm, or with (c) $h_{\text{sup}} = 1.3$ mm are considered. While the grey and dark-grey areas represent the substrate and superstrate, respectively, the black dotted line is the thin-PRS discontinuity represented by X_s. The absolute value of the electric-field leaky-wave mode is reported normalized with respect to its maximum $|E_\rho|_{\max}$ through a solid line vs. z normalized with respect to h_{tot}.

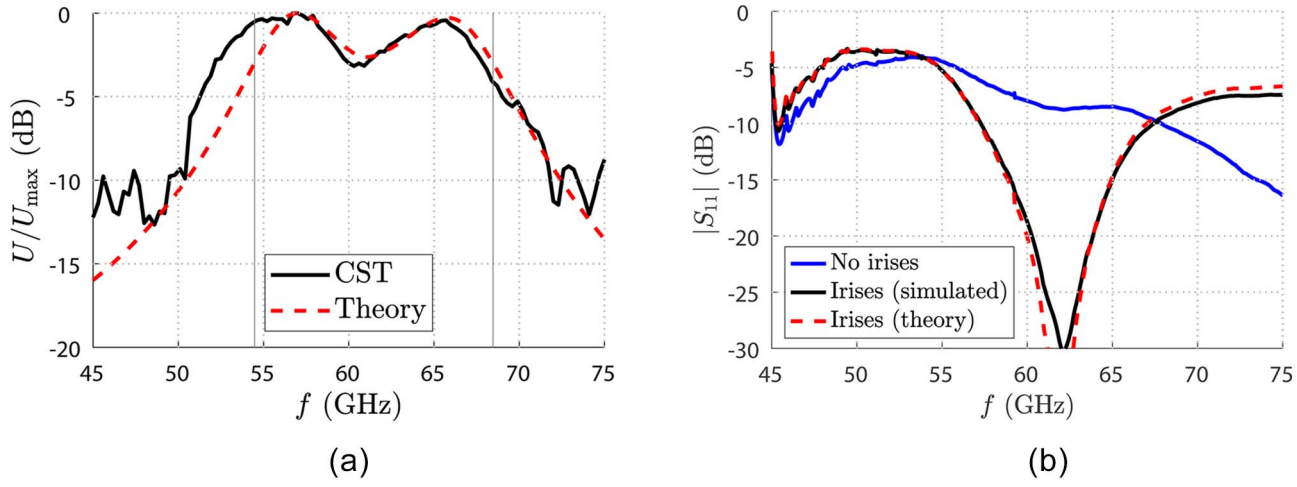


Figure 5. (a) Radiation pattern of a Fabry–Perot cavity antenna based on a thick PRS. Simulated results (black solid line) and theoretical results (red dashed line) are in a good agreement. The vertical solid lines represent the −3 dB power limits. (b) Reflection coefficient of a realistic truncated Fabry–Perot cavity antenna based on a thick PRS and fed through a rectangular waveguide by means of a quasi-resonant slot on the ground plane. By considering a waveguide of length $L_{\text{WG}} = \lambda_0$ (see Fig. 1(b)), the simulated magnitude of the S_{11} parameter is reported when a matching network is not considered (blue solid line) or two optimized capacitive irises are introduced (black solid line). The red dashed line represents the S_{11} parameter predicted by the feeding-network optimization procedure proposed in [17].

Some representative results of the FMT analyses are reported in Fig. 4. The tangential electric-field components, normalized with respect to their maxima, are plotted vs. z, normalized with respect to h_{tot} ($h_{\text{sup}} = 0$ for the FPCA based on a thin PRS). As expected, for a thin-PRS case (see Fig. 4(a)) the tangential electric field follows a sine-like envelope inside the cavity and a typical leaky pattern outside. We note that the value assumed by $|E_\rho|$ at the air-substrate interface strongly depends on the reactance value: a lower X_s generates a lower $|E_\rho(z = z_{\text{sub}})|$ (for the limit case $X_s \to 0$, the tangential electric field tends to zero as in the asymptotic case of a parallel-plate waveguide). It is even more interesting to observe the thick-PRS cases. As preliminarily discussed, a superstrate thickness $h_{\text{sup}} = 0.5$ mm is not enough to achieve a PRS non-Foster behavior (see Fig. 2 and Fig. 3) and, in turn, a bandwidth enhancement. This condition occurs, instead, for $h_{\text{sup}} = 1.3$ mm. This difference is present also for the modal-field distribution obtained through the FMT. As can be inferred by Fig. 4(b) and Fig. 4(c), the bandwidth enhancement in thick PRS is appreciable only for superstrate modes that properly resonate above the cavity. It is worthwhile to point out that this effect occurs only for superstrate thicknesses in the order of $h_{\text{sup}} = \lambda_d/2$.

Full-wave analysis

In order to corroborate the proposed analysis and observe the simulated radiating features of the device, the entire three-dimensional (3-D) model of the FPCA based on the thick PRS with $h_{\text{sup}} = 1.3$ mm has been implemented on CST Microwave Studio [31] assuming a lateral dimension of the device $L = 10\lambda_0$. The latter provides a radiation efficiency of about 99% through the typical formulas of leaky-wave antennas $\eta_r = 1 - e^{-2\pi\hat{\alpha}L/\lambda_0}$ [2], with L being the lateral dimension of the Fabry–Perot cavity (see Fig. 1). (It is worth noting that the considered expression is an underestimation of the actual radiation efficiency due to the effect of the cylindrical radial spreading in 2-D leaky-wave antennas, which is not present in their 1-D counterpart).

Figure 5(a) shows how the normalized far-field radiation pattern at broadside, evaluated through both a theoretical and a simulative approach, evolves for different working frequencies f. By exploiting the leaky-wave theory in [29], it is indeed possible to find the far-field radiation intensity at broadside as a function of the leaky phase and attenuation constants as follows:

https://doi.org/10.1017/S1759078725102432 Published online by Cambridge University Press

Table 1. Design parameters of the feeding network used for matching the thick-PRS-based Fabry–Perot cavity antenna

a	b	d_1	d_2	g_1	g_2
$2\lambda_0/3$	$\lambda_0/3$	$0.2\lambda_0$	$0.1025\lambda_0$	$0.45b$	$0.375b$

$$U(\omega, \theta = 0) = \frac{4\sqrt{\varepsilon_r}U_0}{k_0 h_{\text{sub}}} \left[\frac{\hat{\alpha}\hat{\beta}}{\left(\hat{\alpha}^2 + \hat{\beta}^2\right)^2} \right], \tag{14}$$

where U_0 is a multiplicative excitation constant related to the amplitude of the leaky-wave mode. It is worthwhile to point out that the slight disagreement between theoretical and full-wave results in terms of radiation pattern in Fig. 5(a) are due to the *edge effects* which are present when a realistic, finite-size antenna is considered. In this regard, it is worthwhile to point out that it is also possible to further enlarge the radiation-pattern bandwidth by properly truncating the device (see, e.g., [35, 36]).

As concerns the source, in order to realize a realistic counterpart of an HMD on the ground plane [14], a quasi-resonant slot fed by a rectangular waveguide – with transverse dimensions given by the width a and height b reported in Table 1 – has been considered (see Fig. 1). However, by simply connecting a rectangular-waveguide feeding scheme to the antenna, the device is mismatched in the theoretical bandwidth (see the blue curve in Fig. 5(b)). For this reason, a matching network constituted by two capacitive irises has been designed and implemented on the 3-D model of the device. The choice of the geometrical parameters – i.e., the iris gaps g_1 and g_2 and the distances d_1 and d_2 (see Fig. 1(b)) – has been carried out through an efficient semi-analytical matching technique based on a transmission-line equivalent model. The latter, as shown in [17], only requires a single full-wave simulation of the device by de-embedding the waveguide port of a distance $L_{\text{RW}} = \lambda_0$ (without the guide discontinuities). In particular, once the reflection coefficient and, thus, the device input impedance at the ground-plane level are known, they can be exploited in a transmission-line model to find the best configuration of the considered capacitive irises in a fast numerical manner (since such waveguide discontinuities are represented through well-known closed formulas [37, 38]). By defining the capacitive-irises design parameters as in Fig. 1, the matching network has been implemented on CST Microwave Studio [31] with the feeder dimensions in Table 1. Simulated results obtain a very good reflection-coefficient profile which is in an impressive agreement with the S_{11} theoretically predicted with the approach shown in [17] (see Fig. 5(b)). In this manner, the impedance bandwidth, viz., the working frequencies for which the reflection coefficient is lower than −10 dB, covers almost the overall theoretical bandwidth.

Conclusion

The analysis of Fabry–Perot cavity antennas based on thin and thick partially reflecting sheets has been addressed through a field-matching-technique approach in this paper. A three-dimensional model of the leaky-wave antenna, implemented with the best superstrate height in terms of bandwidth enhancement, has been realized on a full-wave solver and matched through a semi-analytical technique. Theoretical results are in a very good agreement with full-wave simulations, corroborating the effectiveness of the different design steps proposed in this work. As a consequence, this paper lays the groundwork for rapidly optimizing the design parameters of Fabry–Perot cavity antennas based on thick partially reflecting sheets through a simple yet effective approach based on a field matching technique.

Acknowledgements. W. F. acknowledges the support of the CNR-CNPq biennial (2025–2026) bilateral project METASURFANT "Metasurface antennas for high data-rate sub-THz wireless indoor communications". A. G. thanks for the support of the European Union under the Italian National Recovery and Resilience Plan (NRRP) of NextGenerationEU, partnership on "Telecommunications of the Future" (PE00000001 – program "RESTART"). The Authors wish also to thank E. Ballarini for her help in the numerical simulations.

Competing interests. The authors declare none.

References

1. **Negri E, Ballarini E, Fuscaldo W, Burghignoli P and Galli A** (2024) Analysis of leaky modes in Fabry–Perot cavity antennas based on thin and thick partially reflecting sheets. In 54th *European Microwave Conference (EuMC 2024)*, Paris, France, 1–4.
2. **Burghignoli P, Fuscaldo W and Galli A** (2021) Fabry–Perot cavity antennas: The leaky-wave perspective. *IEEE Antennas and Propagation Magazine* **63**(4), 116–145.
3. **Kim D, Ju J and Choi J** (2012) A mobile communication base station antenna using a genetic algorithm based Fabry-Perot resonance optimization. *IEEE Transactions on Antennas and Propagation* **60**(2), 1053–1058.
4. **Hussain N, Jeong M-J, Park J and Kim N** (2019) A broadband circularly polarized Fabry-Perot resonant antenna using a single-layered PRS for 5G mimo applications. *IEEE Access* **7**, 42897–42907.
5. **Muhammad SA, Sauleau R and Legay H** (2011) Small-size shielded metallic stacked Fabry–Perot cavity antennas with large bandwidth for space applications. *IEEE Transactions on Antennas and Propagation* **60**(2), 792–802.
6. **Fuscaldo W, Tofani S, Zografopoulos DC, Baccarelli P, Burghignoli P, Beccherelli R and Galli A** (2018) Systematic design of THz leaky-wave antennas based on homogenized metasurfaces. *IEEE Transactions on Antennas and Propagation* **66**(3), 1169–1178.
7. **Fuscaldo W, Jackson DR and Galli A** (2024) Characterization and comparison of formulas for optimizing broadside radiation and null beams in 2D leaky-wave antennas. *International Journal of Microwave and Wireless Technologies* 1–7.
8. **Guo Y-X, Chia M, Chen ZN and Luk K-M** (2004) Wide-band L-probe fed circular patch antenna for conical-pattern radiation. *IEEE Transactions on Antennas and Propagation* **52**(4), 1115–1116.
9. **Mateo-Segura C, Feresidis AP and Goussetis G** (2013) Bandwidth enhancement of 2-D leaky-wave antennas with double-layer periodic surfaces. *IEEE Transactions on Antennas and Propagation* **62**(2), 586–593.
10. **Feresidis A and Vardaxoglou J** (2001) High gain planar antenna using optimised partially reflective surfaces. *IEE Proceedings – Microwaves, Antennas and Propagation* **148**(5), 345–350.
11. **Burghignoli P, Lovat G, Capolino F, Jackson DR and Wilton DR** (2008) Modal propagation and excitation on a wire-medium slab. *IEEE Transactions on Microwave Theory and Techniques* **56**(5), 1112–1124.
12. **Burghignoli P, Lovat G, Capolino F, Jackson DR and Wilton DR** (2010) Highly polarized, directive radiation from a Fabry-Pérot cavity leaky-wave antenna based on a metal strip grating. *IEEE Transactions on Antennas and Propagation* **58**(12), 3873–3883.
13. **Tumbaga C** (2020) Modernizing mm-wave measurements with 110 GHz coaxial components. *Microwave Journal* **63**(10), 98–102.
14. **Negri E, Fuscaldo W, Burghignoli P and Galli A** (2023) Leaky-wave analysis of TM-, TE-, and hybrid-polarized aperture-fed Bessel-beam launchers for wireless power transfer links. *IEEE Transactions on Antennas and Propagation* **71**(2), 1424–1436.
15. **Negri E, Fuscaldo W, González-Ovejero D, Burghignoli P and Galli A** (2024) TE-polarized leaky-wave beam launchers: Generation of Bessel and Bessel–Gauss beams. *Applied Physics Letters* **125**(18), 181703.
16. **Taillieu J, Pascual AJ, Pakovic S, Morvan X, Fuscaldo W, Ettorre M and González-Ovejero D** (2025) High-data-rate and resilient wireless links at

https://doi.org/10.1017/S1759078725102432 Published online by Cambridge University Press

W-band enabled by all-metal spline horns. *IEEE Transactions on Antennas and Propagation* **73**(3), 1834–1839.
17. **Negri E, Fuscaldo W, Tofani S, Burghignoli P and Galli A** (2024) An efficient and accurate semi-analytical matching technique for waveguide-fed antennas. *Scientific Reports* **14**(1), 3892.
18. **Tretyakov S**, (2003) *Analytical Modeling in Applied Electromagnetics*., Norwood, MA, USA: Artech House.
19. **Luukkonen O, Simovski C, Granet G, Goussetis G, Lioubtchenko D, Raisanen AV and Tretyakov SA** (2008) Simple and accurate analytical model of planar grids and high-impedance surfaces comprising metal strips or patches. *IEEE Transactions on Antennas and Propagation* **56**(6), 1624–1632.
20. **Fuscaldo W, Maita F, Maiolo L, Beccherelli R and Zografopoulos DC** (2024) Broadband terahertz characterization and electromagnetic models for fishnet metasurfaces: From the homogenization to the resonant regime. *IEEE Transactions on Antennas and Propagation* **72**(8), 6771–6776.
21. **Zhao T, Jackson D, Williams J and Oliner A** (2005) General formulas for 2-D leaky-wave antennas. *IEEE Transactions on Antennas and Propagation* **53**(11), 3525–3533.
22. **Jackson DR, Caloz C and Itoh T** (2012) Leaky-wave antennas. *Proceedings of the IEEE* **100**(7), 2194–2206.
23. **von Trentini G** (1956) Partially reflecting sheet arrays. *IRE Transactions on Antennas and Propagation* **4**(4), 666–671.
24. **Foster RM** (1924) A reactance theorem. *Bell System Technical Journal* **3**(2), 259–267.
25. **Lv Y-H, Ding X and Wang B-Z** (2019) Dual-wideband high-gain Fabry–Perot cavity antenna. *IEEE Access* **8** 4754–4760.
26. **Hosseini A, Capolino F, De Flaviis F, Burghignoli P, Lovat G and Jackson DR** (2014) Improved bandwidth formulas for Fabry-Pérot cavity antennas formed by using a thin partially-reflective surface. *IEEE Transactions on Antennas and Propagation* **62**(5), 2361–2367.
27. **Al-Tarifi MA, Anagnostou DE, Amert AK and Whites KW** (2013) Bandwidth enhancement of the resonant cavity antenna by using two dielectric superstrates. *IEEE Transactions on Antennas and Propagation* **61**(4), 1898–1908.
28. **Hosseini A, De Flaviis F and Capolino F** (2016) Design formulas for planar Fabry–Pérot cavity antennas formed by thick partially reflective surfaces. *IEEE Transactions on Antennas and Propagation* **64**(12), 5487–5491.
29. **Almutawa AT, Hosseini A, Jackson DR and Capolino F** (2019) Leaky-wave analysis of wideband planar Fabry–Pérot cavity antennas formed by a thick PRS. *IEEE Transactions on Antennas and Propagation* **67**(8), 5163–5175.
30. **Sorrentino R and Mongiardo M** (2005) *Transverse Resonance Techniques*., New York, NY, USA: John Wiley & Sons, Ltd.
31. CST products Dassault Systèmes, France, 2021. [Online]. Available: http://www.cst.com.
32. **Galdi V and Pinto MI** (2000) A simple algorithm for accurate location of leaky-wave poles for grounded inhomogeneous dielectric slabs. *Microwave and Optical Technology Letters* **24**(2), 135–140.
33. **Lovat G, Burghignoli P and Jackson DR** (2006) Fundamental properties and optimization of broadside radiation from uniform leaky-wave antennas. *IEEE Transactions on Antennas and Propagation* **54**(5), 1442–1452.
34. **Ip A and Jackson DR** (1990) Radiation from cylindrical leaky waves. *IEEE Transactions on Antennas and Propagation* **38**(4), 482–488.
35. **Baba AA, Hashmi RM and Esselle KP** (2017) Achieving a large gain-bandwidth product from a compact antenna. *IEEE Transactions on Antennas and Propagation* **65**(7), 3437–3446.
36. **Baba AA, Hashmi RM, Esselle KP and Weily AR** (2018) Compact high-gain antenna with simple all-dielectric partially reflecting surface. *IEEE Transactions on Antennas and Propagation* **66**(8), 4343–4348.
37. **Collin RE**, (1990) *Field Theory of Guided Waves*., Hoboken, NJ, USA: John Wiley & Sons.
38. **Marcuvitz N**, (1951) *Waveguide Handbook*, New York: IET, 21.



Edoardo Negri was born in Orvieto, Italy, in 1997. He received the B.Sc. and M.Sc. degrees (cum laude) in electronic engineering, with honorable mention for the academic curriculum, from Sapienza University of Rome, Rome, Italy, in July 2019 and 2021, respectively, where he received, in January 2025, the Ph.D. degree (cum laude and the 'Doctor Europaeus' label) in Information and Communications Technologies (applied electromagnetics curriculum). From March to May 2023, he was a Visiting Ph.D. Student with the Institut d'Électronique et de Télécommunications de Rennes (IETR), Université de Rennes 1, Rennes, France. From September to November 2023, he was a visiting Ph.D. Student in Ferdinand-Braun-Institut, Leibniz-Institut fchstfrequenztechnik (FBH), Berlin, Germany. Since July 2024, Dr. Negri has been a Research Fellow at the Institute for Microelectronics and Microsystems (IMM) of the National Research Council (CNR), Rome, Italy. His main research interests include leaky waves, metasurfaces, focusing devices, wireless near-field links at high frequencies (ranging from microwaves to terahertz), and THz devices. Dr. Negri received the "Antonio Ventura" Award as one of the best engineering students at the Sapienza University of Rome in 2022, the IEEE Antennas and Propagation Society (APS) Fellowship Award in 2023, the European Microwave Association (EuMA) Internship Award in 2023, an honorary mention in the "Barzilai Award" at the "Riunione Nazionale di Elettromagnetismo (RiNEm)" 2024, the second prize for the industrial call for ideas "Huawei TechArena", and the first prize at the "Best Student Paper Award" at the International Symposium on Antennas and Propagation (ISAP) in 2024. He is currently a Guest Editor of the journal Symmetry (MDPI).



Walter Fuscaldo received the M.Sc. (cum laude) degree in Telecommunications Engineering from Sapienza University of Rome, Rome, in 2013. In 2017, he received the Ph.D. degree (cum laude and with the Doctor Europaeus label) in Information and Communication Technology (Applied Electromagnetics curriculum) from both the Department of Information Engineering, Electronics and Telecommunications (DIET), Sapienza University of Rome, and the Institut d'Électronique et de Télécommunications de Rennes (IETR), Université de Rennes 1, Rennes, France, under a cotutelle agreement between the institutions. In 2014, 2017, 2018, he was a Visiting Researcher and in 2023 a Visiting Scientist with the NATO-STO Center for Maritime Research and Experimentation (CMRE), La Spezia, Italy. In 2016, he was a Visiting PhD student with the University of Houston, Houston, TX, USA. From July 2017 to June 2020, he was a Research Fellow at Sapienza University of Rome, and in July 2020, he joined the Institute for Microelectronics and Microsystems (IMM), Rome of the National Research Council of Italy as a Researcher, where he is currently a Senior Researcher since 2023. His current research interests include propagation of leaky, surface, and plasmonic waves, analysis and design of leaky-wave antennas, generation of electromagnetic localized waves, THz technology and spectroscopy, graphene electromagnetics, and metasurfaces. Dr. Fuscaldo was awarded several prizes, among which is the prestigious EuRAAP Leopold B. Felsen Award for Excellence in Electrodynamics in 2025. Since 2021 he has been included in the World's Top 2% Scientists' list by Stanford University. He is currently an Associate Editor of the journals Nature – Scientific Reports, IET – Microwaves, Antennas and Propagation, and IET – Electronics Letters.

https://doi.org/10.1017/S1759078725102432 Published online by Cambridge University Press



Paolo Burghignoli was born in Rome, Italy, on February 18, 1973. He received the Laurea degree (cum laude) in electronic engineering and the Ph.D. degree in applied electromagnetics from the La Sapienza University of Rome, Rome, in 1997 and 2001, respectively. In 1997, he joined the Electronic Engineering Department and is currently with the Department of Information Engineering, Electronics and Telecommunications, La Sapienza University of Rome. From January 2004 to July 2004, he was a Visiting Research Assistant Professor with the University of Houston, Houston, TX, USA. From November 2010 to October 2015, he was an Assistant Professor with the La Sapienza University of Rome, where he has been an Associate Professor since November 2015. In March 2017, he received the National Scientific Qualification for the role of a Full Professor of electromagnetic fields in Italian Universities. He is currently teaching courses of electromagnetic fields, advanced antenna engineering, and analytical techniques for wave phenomena for the B.Sc., M.Sc., and Ph.D. programs in the ICT area with La Sapienza University. He has authored about 250 articles in international journals, books, and conference proceedings. His research interests include the analysis and design of planar antennas and arrays, leakage phenomena in uniform and periodic structures, numerical methods for integral equations and periodic structures, propagation and radiation in metamaterials, electromagnetic shielding, transient electromagnetics and graphene electromagnetics. Dr. Burghignoli was a recipient of the "Giorgio Barzilai" Laurea Prize from 1996 to 1997 presented by the former IEEE Central and South Italy Section, the 2003 IEEE MTT-S Graduate Fellowship, and the 2005 Raj Mittra Travel Grant for junior researchers presented at the IEEE AP-S Symposium on Antennas and Propagation, Washington, DC. He is a coauthor of the "Fast Breaking Papers, October 2007" in EE and CS, about metamaterials (paper that had the highest percentage increase in citations in Essential Science Indicators). He was a Secretary of the 12th European Microwave Week (EuMW 2009) and a member of the Scientific Board and Local Organizing Committee of the 41st PhotonIcs and Electromagnetics Research Symposium (PIERS 2019). In 2017, 2020, and 2021 the IEEE Antennas and Propagation Society recognized him as an outstanding reviewer for the IEEE TRANSACTIONS ON ANTENNAS AND PROPAGATION. He is currently serving as an Associate Editor of the Electronics Letters (IET) the International Journal of Antennas and Propagation (Wiley). He is a Senior Member of the IEEE



Alessandro Galli received the Laurea degree in Electronics Engineering and the Ph.D. degree in Applied Electromagnetics from Sapienza University of Rome, Rome, Italy. Since 1990 he has been with the Department of Information Engineering, Electronics and Telecommunications at Rome Sapienza. He became an Assistant Professor and an Associate Professor in the sector of Electromagnetic Fields in 2000 and 2002, respectively. In 2013 he obtained the National Scientific Qualification, and later he definitively achieved the role of Full Professor in the same sector. His research interests concern various topics of guided-wave and radiation theory and applications, ranging from microwaves to terahertz. His activities also include topics of geoelectromagnetics, bioelectromagnetics, and plasma heating. He is the author of over 300 papers in international journals, books, and conference proceedings. Prof. Galli was elected Italian Representative in the Board of Directors of the European Microwave Association (EuMA) from 2010 to 2015. He was General Co-Chair of the 2014 European Microwave Week. Since 2024 he has been elected representative of Sapienza University of Rome Unit of the Italian Society of Electromagnetism (SIEm). He received various awards and recognitions for his research activity: in 2017 he was elected Best Teacher of the courses of the European School of Antennas (ESoA).

https://doi.org/10.1017/S1759078725102432 Published online by Cambridge University Press